Sensors & Transducers, Vol. 27, Special Issue, May 2014, pp. 209-216

www.sensorsportal.com

Sensors & Transducers

http://www.sensorsportal.com

Charge Carrier Transport Properties of Vacuum Evaporated Anthrylvinylbenzene Thin Films

Haikel HRICHI, Maha BENZARTI-GHEDIRA, Nejmeddine JABALLAH, Rafik BEN CHAABANE, Mustapha MAJDOUB, Hafedh BEN OUADA

Laboratoire d'Interfaces et Matériaux Avancés (LIMA),
Université de Monastir Faculté des Sciences de Monastir,
Bd. de l'Environnement, 5019 Monastir, Tunisie
Tel.: + 216 99 954 254, fax: 216 73 500 278
E-mail: haikelhrichi@gmail.com

Received: 23 November 2013 /Accepted: 12 January 2014 /Published: 26 May 2014

Abstract: The charge carrier conduction processes and dielectric properties of two new materials based on anthracene core structure, 1-(9 anthrylvinyl)-4-benzyloxybenzene (AVB) and 1,4-bis(9-anthrylvinyl)benzene (AV2B) diodes have been investigated using dc current density–voltage (*J–V*) and AC impedance spectroscopy (100Hz–10MHz). The DC electrical properties of ITO/anthracene derivative /Al device showing an ohmic behavior at low voltages and switches to space charge limited current (SCLC) conduction with exponential trap distribution at higher voltages. The best performance device was achieved from ITO/AVB/Al structure showing the high charge carrier mobility which has also been evaluated from SCLC as 6.55×10^{-6} cm/Vs. According to the impedance spectroscopy results the structures were modeled by equivalent circuit designed as a parallel resistor R_p and capacitor C_p network in series with resistor R_s. The evolution of the electrical parameters with frequency and bias voltage of these anthracene-based systems has been discussed. The conductivity $\sigma(\omega)$ evolution with frequency and bias voltage was studied for ITO/anthracene derivatives/Al devices. The dc conductivity σ_{dc} for these devices has been determined. The ac conductivity σ_{ac} showed a variation in angular frequency as $A.\omega^s$ with a critical exponent $s < 1$ suggesting a hopping conduction mechanism at high frequency.

Keywords: Anthracene derivatives, *J–V* characteristics, Space charge limited current, Impedance spectroscopy.

1. Introduction

Organic π-conjugated derivatives have recently a great interest as semi-conducting materials and have been successfully applied in different organic electronic devices such as organic light emitting diodes (OLEDs) [1, 2], thin film transistors (TFTs) and solar cells [3–6]. In fact, such organic functional materials offer numerous advantages like low-cost, easy processing (e.g. spin-coating, ink-jet, evaporation) and good compatibility with flexible plastic substrates. Furthermore, molecular electronic devices are being recently a key subject in nanotechnology developments.

Anthracene was one of the first aromatic materials employed in OLED elaboration. The first experiments were carried out by Pope in the early 1960s [7]. Soon after, several reports on single-crystal anthracene-based OLEDs were published [8, 9], and good quantum yields were obtained (up to

5 %). Nevertheless, such devices are thick and hence require very high operating voltage (over 100 V). The improvement in the operating voltage was achieved by vacuum evaporating thin layers of anthracene; in this case the operating voltage was lowered up to 30 V [10]. Currently, anthracene and its derivatives were much investigated [11] and frequently used in OLEDs [12], as well as in other organic thin-layer-based electronic devices such as Organic thin-film transistors (OTFTs) [4] transistors and photovoltaic cells [13]. Tuning the opto-electronic properties of such derivatives has become nowadays possible due to the drastic development of chemical technology. On the one hand, effective synthetic strategies are now available. On the other hand, it is a challenge to address and influence the electronic properties of the conjugated backbone from the outside via specific interactions of covalently attached functional groups with external chemical or physical stimuli. Hence, there is a clear need to control and improve their solid state charge transporting properties for achieving device optimization. Thus, there are increasing interests in studying the relationship between the charge transporting properties of π-conjugated organic materials and their molecular structures. Attractive non bonded interactions between aromatic rings are seen in many areas of chemistry and recently in physics when conjugated polymers are studied, and hence are of interest to all realms of chemistry and physics [14].

In this work, we report the electrical properties investigation of two new anthracene-based conjugated molecules. The device investigated consist of the indium-tin-oxide (ITO) acting as a transparent hole injecting electrode on to which, the AVB and AV2B was deposed by evaporation under vacuum as well as for the Al on top acting as electron injecting electrode. The thickness of the organic film was estimated to be 350 nm. Our investigations of the ITO/AVB/Al and ITO/AV2B/Al diodes are focused on the electrical and carrier transport properties. First we present the experimental current density-voltage *(J–V)* characteristic of the device model, second we studied impedance spectroscopy (IS). After that, we discuss different regimes of conduction of the current, and finally, we give the equivalent circuit model.

2. Experimental: Sample Preparation and Characterization

This work is based on two new anthracene-core conjugated systems (Fig. 1), 1-(9-anthrylvinyl)-4-benzyloxybenzene (AVB) and 1,4-bis(9-anthryl-vinyl)benzene (AV2B), whose synthesis has been reported in previous work [10].

The devices in our study consist of a single organic layer sandwiched between two electrodes on top of a glass substrate (Fig. 2). They were fabricated on ITO-coated glass substrates (Merck Display Technologies, Ltd.) with a sheet resistance of 13 Ω/square, used as anode. The organic layer were deposited by thermal evaporation under a vacuum of $5*10^{-6}$ Torr, which is a technique compatible with integrated circuit technology and the fabrication of surfaces with uniform morphology. The evaporation temperature was maintained at about 270–280 °C and the evaporation rate (0.5 nm/s) and the deposited film thickness (350 nm) is controlled by a piezoelectric quartz crystal microbalance [15].

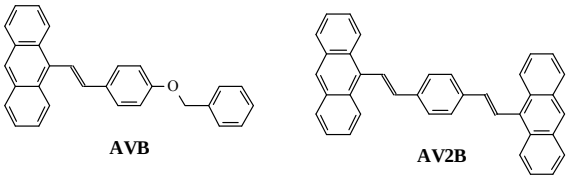

Fig. 1. Chemical structure of anthracene derivatives.

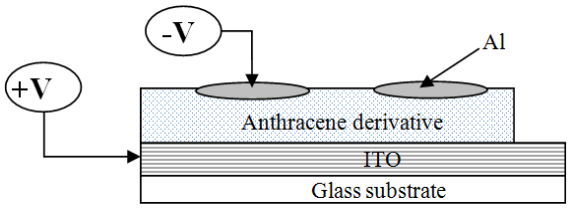

Fig. 2. ITO/anthracene derivative/Al diode heterostructure.

The substrate was pre-cleaning successively for 20 min in acetone and isopropyl alcohol in an ultrasonic bath and finally dried by a nitrogen gas flow. Such pre-cleaning process ensures an ITO substrate of good quality with reduced roughness without any glass fragments (due to cutting of small devices) and organic contaminants or any residual humidity. Then, the anthracene derivative was evaporated onto the ITO electrode. In order to study the transport properties an aluminium contact was evaporated, as a top electrode, at a pressure below 10^{-6}Torr. The active areas of the diodes are approximately 3.14×10^{-2} cm^2.

The current–voltage characteristics of the ITO/anthracene derivative/Al devices were measured from an applied bias of -5 to 5 V by using a Keithley 236 source measure unit. The diode structure studied is a metal/polymer/metal consisting of indium tin oxide as positive contact and an Aluminium electrode as the negative contact as shown in Fig. 2. The ac measurements were performed with an HP 4192A LF impedance analyzer. In general, the excitation potential for ac measurements is given by:

$$V = V_0 + V_{\text{mod}} \sin(\omega t), \quad (1)$$

where V_0 is the DC bias, V_{mod} is the oscillation level and $\omega/2\pi$ is the frequency. In our case, the measurements were performed under the following

conditions: a signal magnitude of 50 mV was used over a frequency range of 100–10 MHz using a computer controlled HP 4192A LF. All these measurements were performed in the dark and at room temperature.

3. Results and Discussion

3.1. DC Study: Current Density-voltage Characteristics

The electrical transport properties are important in optoelectronic devices. The transport of charges has been investigated using current density-voltage (*J–V*) measurements in indium tin oxide: ITO/AVB/Al and ITO/AV2B/Al diode structures (Fig. 3).

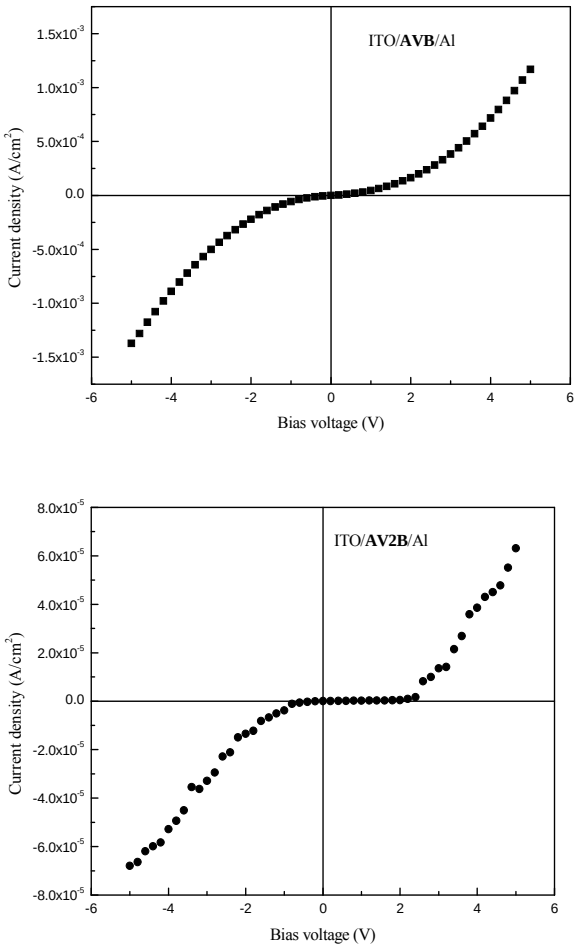

Fig. 3. The J-V characteristics of ITO/AVB/Al and ITO/AV2B/Al devices.

The *J-V* curve shows a typical diode response in both forward and reverse bias. The current values obtained for AVB is two decades higher than measured for AV2B. This difference is attributed to the morphology quality of the two films. Indeed, the presence of crystalline zones in the AVB film enhances their conductive properties [10]. Moreover, the nature of the side group demonstrates that benzyloxy group incorporated in the AVB derivative can give rise to distinct morphological characteristics, impacting its electrical behavior and it can be useful in the control of the π-π stacking of rigid conjugated olygomers. It is well established that an increase in the number of benzene groups leads to an increase in conductivity in a conjugated system because of π-π-stacking phenomenon [14]. However, the AVB olygomer, which has the lowest number of benzene groups, has a greater conductivity than the AV2B olygomer. This behavior can be explained by the presence of crystalline regions in the first material while the second is completely amorphous [10]. The density of charge carriers (p_0), turn-on voltages (V_{on}) and effective mobility (μ) are extracted and are presented in Table 1. The asymmetric *J-V* characteristic at higher voltages is attributed to the difference of injection barriers to electrons and holes due to different work functions for the ITO anode (4.7 eV) and the Al cathode (4.3 eV).

The *J-V* characteristic in log-log plots of ITO /anthracene derivatives /Al is shown in Fig. 4.

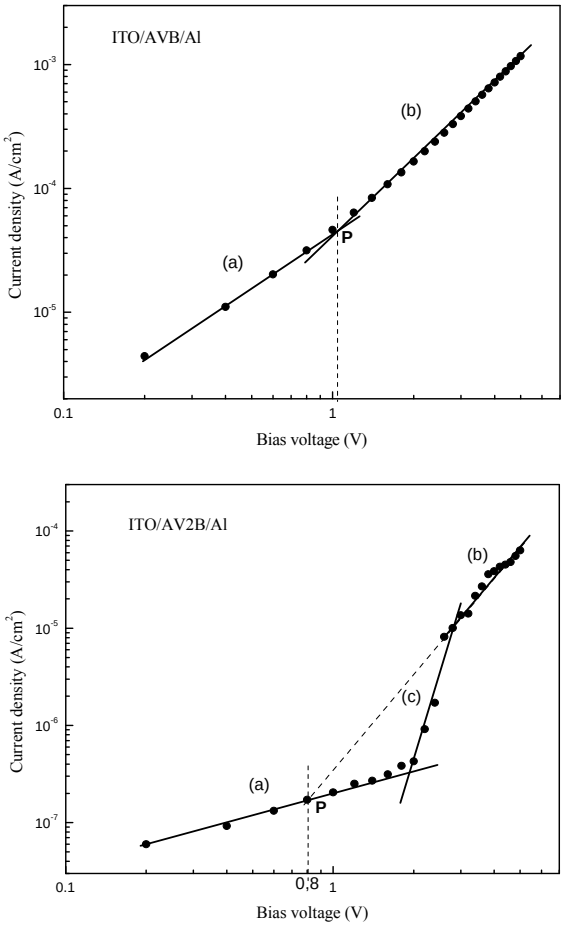

Fig. 4. The log–log of the J-V characteristics of ITO/AVB/Al and ITO/AV2B/Al devices.

The current dependence of applied voltage appears to follow a power law ($J \propto V^m$) with three regimes corresponding to:

At low bias voltage, the current increases linearly with voltage for the two devices, which indicates an ohmic conduction ($J \propto V$) (segment a). For this regime, the current density is described by [16]:

$$J_{\Omega} = qp_0\mu\frac{V}{d}, \quad (2)$$

where q is the electronic charge, μ is the charge carrier mobility, p_0 is the free carrier density, V is the applied voltage, and d is the film thickness.

In the second regime, for medium bias voltage (segment c), the current density increases rapidly with voltage and it is described by $J \propto V^{m+1}$. This is attributed to SCLC conduction mechanism limited by distributed traps since the injected charge carriers will fill the traps of the material [17]. In this region, the current increases in a power law ($J \propto V^{10}$) and it is observed only for the ITO/AV2B/Al structure.

At higher bias, all traps are full and the current density depends quadratically on the voltage ($J \propto V^2$) (segment b). This behavior is characteristic of space-charge limited current (SCLC), in which case the current density in the absence of traps in the organic film can be written as [18, 19]:

$$J_{SCLC} = \frac{9}{8}\varepsilon_0\varepsilon_r\mu\frac{V^2}{d^3}, \quad (3)$$

where ε_r is the organic material permittivity and ε_0 is the permittivity of vacuum.

The mobility is one of the most relevant parameters to select the materials used in the production of optoelectronic devices. Indeed, the performance of the device depends on the mobility which governs the recombination between holes (injected at the anode) and electrons (injected at cathode) in the organic diodes. They are different technique to estimated the value of mobility such as Time of flight method (TOF) [20, 21], Fieled-Effect Transistor Configuration (FET) [22] and Space Charge Limited Conduction (SCLC) mechanism [23, 24]. In this work, the hole mobility of the materials has also been evaluated from SCLC theories. In order to determine the dependence of mobility versus the density of charge carriers, we can define the bias voltage V_{tr} from which the J–V characteristic transform into the SCLC regime, is given by [25]:

$$V_{tr} = \frac{8}{9}qp_0\frac{d^2}{\varepsilon_0\varepsilon_r}, \quad (4)$$

by taking $\varepsilon_r \approx 3$ and d thickness film, p_0 is the density of thermally generated charge carrier.

In Table 1, we present extrapolated parameters from J–V characteristics for the two devices. The values of holes mobility is 6.55 10^{-6} cm/Vs (AVB) and 3.03×10^{-8} cm/Vs (AV2B). We believe that our materials are good candidates for optoelectronic applications such as photovoltaic cells, OLEDs and organic transistors.

Table 1. Electrical parameters for ITO/AVB/Al and ITO/AV2B/Al devices from J-V characteristics.

Device structure	ITO/AVB/Al	ITO/AV2B/Al
V_{on} (V)	2.27	2.73
p_0(cm^2/V.s)	1.58×10^{15}	1.21×10^{15}
μ_p(cm^2/Vs)	6.55×10^{-6}	3.03×10^{-8}

3.2. AC Study: Impedance Spectroscopy

Impedance spectroscopy has shown to be a useful tool to understand the transport mechanisms and interface processes in different organic electronics and optoelectronics components (OLEDs) [26, 27].

It is clear from Fig. 5 that the evolution of conductivity σ increases with increasing both frequency and bias voltages. As can be seen, at low frequency the conductivity σ_{dc} at ($\omega \rightarrow 0$) remains constant. However, after a critical frequency (f_c), the conductivity σ_{ac} starts to increase with increasing the frequency. Indeed, for ac conductivity, the charge carrier will hop from a site i to another site j (during τ_H) where it will relax during τ_0 (related to AC electrical parameters of the previous section).

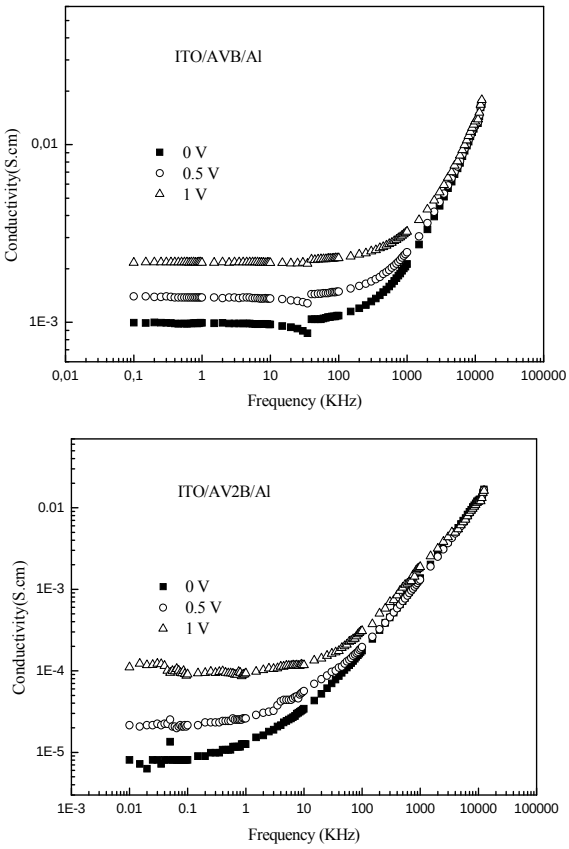

Fig. 5. Frequency dependence of the conductivity σ (ω) for ITO/AVB/Al and ITO/AV2B/Al at different bias voltages.

Therefore, the frequency dependence of conductivity can be expressed by the following equation [29, 31]:

$$\sigma = \sigma_{dc} + \sigma_{ac}(\omega) = \sigma_{dc} + A\omega^{s}, \quad (5)$$

where σ_{dc} is the dc electrical conductivity, $\sigma_{ac}(\omega)$ is the ac conductivity, ω is the angular frequency of the applied excitation, A is the dispersion parameter and s the dimension less critical exponent $0 < s < 1$ characterizing hopping conduction.

This is a typical behaviour for a wide variety of materials and is called by Jonscher universal dynamic response (UDR) [32]. The characteristic frequency corresponding to the onset of the conductivity dispersion is known as the hopping frequency, f_H [33], and can be identified as the frequency at which

$$\sigma = 2\sigma(0), \quad (6)$$

By fitting the plot of Fig. 5 (at 0 *V*), after extracting A and s, we have obtained f_H from the universal law:

$$f_H = (\sigma_{dc}/A)^{1/s}, \quad (7)$$

Then, for AVB and AV2B, we have deduced the hopping relaxation time (at 0 volt):

$$\tau_H = (1/f_H), \quad (8)$$

We summarize in Table 2 the hopping conduction parameters at 0 *V* for (σ_{dc}, A, s, f_H and τ_H):

Knowing that τ_0 and τ_H are respectively the time spent by the charge carrier to relax in a site i and the time to jump from site i to site j, the best conductive material will have the lowest sum ($\tau_0 + \tau_H$) which is the case of the ITO/AVB/Al device (Table 2). In fact, this behaviour confirms the obtained results of the static electrical characterizations.

Table 2. Ac electrical and hopping parameters f or ITO/anthracene derivative/Al devices derived from the impedance spectroscopy study at 0 volt.

Device structure	ITO/AVB/Al	ITO/AV2B/Al
R_s (Ω)	331	785
C_p (nF)	29	40
R_p (MΩ)	0.905	108.54
f_0 (kHz)	33.657	0.176
τ_0 (ms)	0.03	5.68
S	1.02306	0.95029
σ_{dc} (S m^{-1})	0.00098	0.00001
A (S m^{-1} rad^{-1})	9.6611E-7	1.9474E-6
f_H (Hz)	867.838	5.593
τ_H (ms)	1.15	178.77
$\tau_0 + \tau_H$(ms)	1.18	184.45

Fig. 6 shows the frequency-dependent real (Z') and imaginary (Z'') part of the impedance for all the two devices without bias. It is observed that the magnitude of Z' decreases with the increase of frequency for all the devices. The curves also display the single relaxation process and indicate an increase in ac conductivity with frequency. The *Z''* reaches a maximum peak $Z''_{max}(\omega_{max})$ for all the devices at different frequencies .This also indicate the single relaxation process in the system.

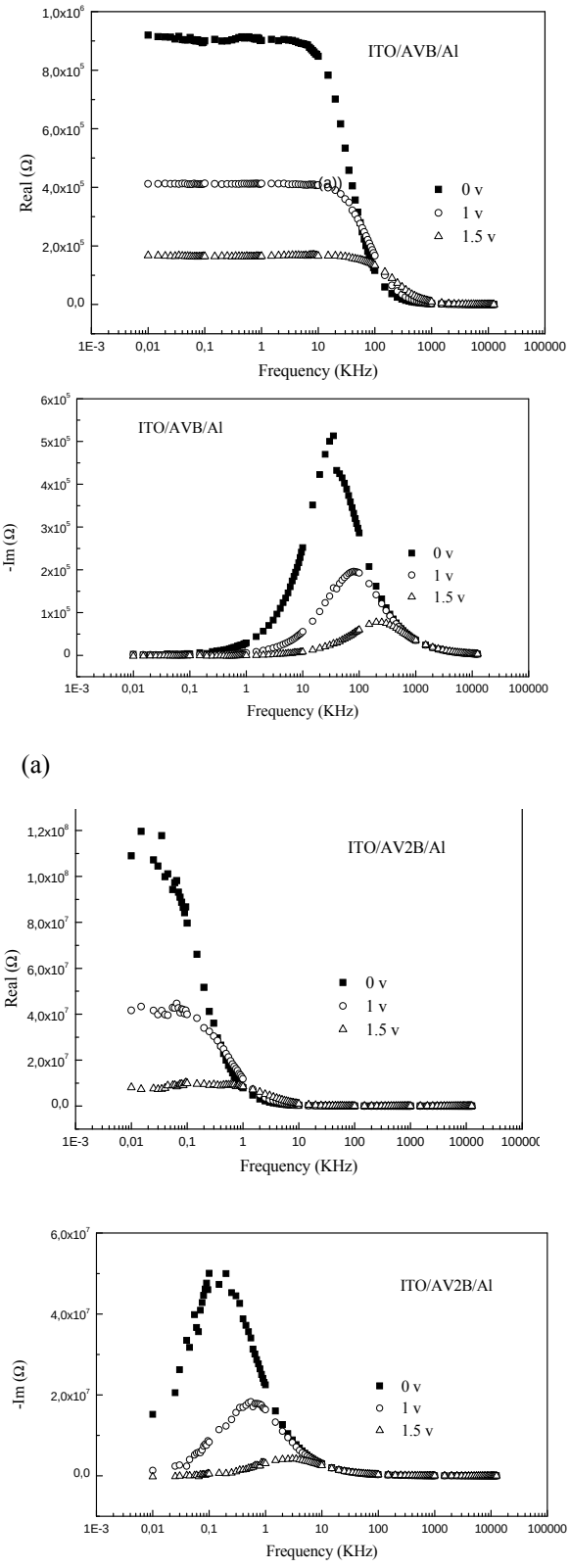

Fig. 6. The frequency dependent real and imaginary part of the impedance for (a) ITO/AVB/Al and (b) ITO/ AV2B /Al at different bias voltages.

Fig. 7 shows the impedance Cole–Cole plots of ITO/AVB/Al diode structure. This plot shows a single semicircle close to the origin which decreases in size with increasing bias. The minimum Re (Z) value observed at high frequencies represents the existence of a series resistance R_s to the capacitor C_p. The maximum Re (Z) value at low frequencies corresponds to the summation of the series resistance R_s and the parallel resistance R_p to the capacitor C_p.

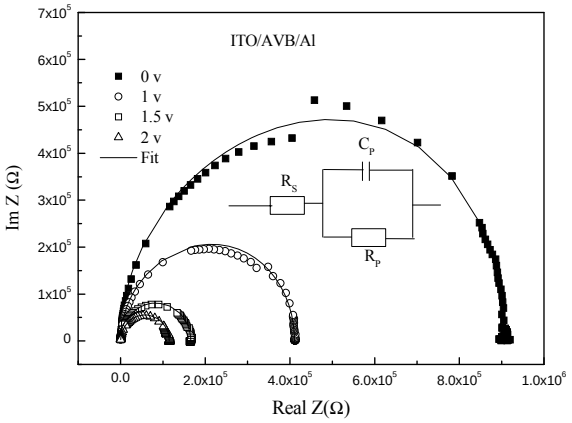

Fig. 7. Cole–Cole plots of complex impedance with a variation of bias voltages in ITO/**AVB**/Al. Symbols are experimental results and lines are fits according to the equivalent circuit.

The impedance spectra were fitted by the following equation [34]:

$$Z(\omega) = R_s + \frac{R_p}{1 + jR_pC_p\omega}, \qquad (9)$$

We plotted the data in log–log scale (Fig. 8). The slopes are obtained 0.5 and 0.6 for two devices at 0 volt. It suggests a single characteristic relaxation time. It suggests a single characteristic relaxation time [35, 36]. The single semi circle is observed with calix[n]arene derivatives[37], anthracene derivatives [10], PPV derivatives[38] and Alq3 device [39].

The impedance of the equivalent circuit is given by:

$$Z(\omega) = \mathrm{Re}(Z) + j\,\mathrm{Im}(Z) = Z' + jZ'', \qquad (10)$$

$$\mathrm{Re}(Z) = R_s + \frac{R_p}{1 + R_p^{\,2}C_p^{\,2}\omega^2} = R_s + \frac{R_p}{1 + (\omega/\omega_0)^2}, \qquad (11)$$

$$-\mathrm{Im}(Z) = \frac{R_p^{\,2}C_p\omega}{1 + R_p^{\,2}C_p^{\,2}\omega^2} = \frac{R_p\omega/\omega_0}{1 + (\omega/\omega_0)^2}, \qquad (12)$$

where ω is the angular frequency of the ac excitation and $\omega_0 = 1/C_pR_p$ is the proper angular frequency of the equivalent electrical circuit. Eliminating the angular frequency we obtain the following equation relation:

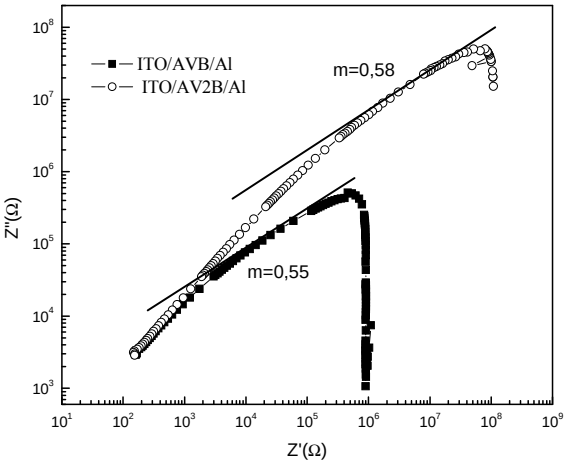

Fig. 8. The Cole–Cole plots of ITO/AVB/Aland ITO/A2VB/Al at 0 volt (in log-log representation).

$$\left[\mathrm{Re}(Z) - (R_s - \frac{R_p}{2})\right]^2 + \mathrm{Im}(Z)^2 = \frac{R_p^{\,2}}{4}, \qquad (13)$$

This equation defines a circle centered at (R_s + R_p/2, 0) with radius R_p/2. Consequently, the equivalent circuit in ac regime represented in the inset of Fig. 7 can be designed as a resistance R_p (due to relaxation losses inside the active material) in parallel with a capacitance C_p (due to charge carrier injection into the material bulk) associated with a resistance R_s in series.

The minimum Re(Z) value observed at high frequencies represents a series resistance R_s which is bias and frequency independent and should be attributed to the hole injecting ITO/anthracene derivatives interface which can be regarded as ohmic. The resistance R_s is about 331 Ω and 785 Ω for AVB and AV2B, respectively, for 0 V. The maximum Re(Z) value at low frequencies represents the addition of a series resistance R_s and a parallel resistance R_p to the capacitance. The resistance R_p is strongly bias dependent. The parameters of the equivalent circuit have been calculated by fitting the experimental impedance spectroscopy data (Fig. 9).

The peak frequency, ω_p, of the Cole–Cole plots for different structures shifts to the higher frequencies when the bias voltage is increased from 0 to 1.5 V (Fig. 8). The peak frequency of the semicircle satisfies the relation $\omega_p.\tau_0$ = 1, where τ_0 is the dielectric relaxation time. τ_0 values (~ ms) indicate that the type of relaxation is dipolar. We showed that the relaxing times, decreases with the increase in the bias voltage, of AVB compound is lower than that of AV2B.

The variations of the fitting parameters of ITO/AVB/Al are shown in Fig. 9. The same behavior is observed for AV2B. Bulk resistance R_p is decreasing with increasing bias voltage which is due to the increase in the number of injected carrier in to the material and the bulk capacitance C_p is almost independent of the applied bias indicating that despite

the level of injected charge, the device still effectively acts as a simple parallel plate capacitor.

The independence of C_p with applied bias is exactly the behavior expected for the SCLC mechanism. From the space charge limited current (SCLC) with an exponential trap distribution theory, the voltage dependent current density is given by the relation [40].

$$J = KV^{m+1} / d^{2m+1}, \quad (14)$$

where d is the thickness of the film and K is the constant.

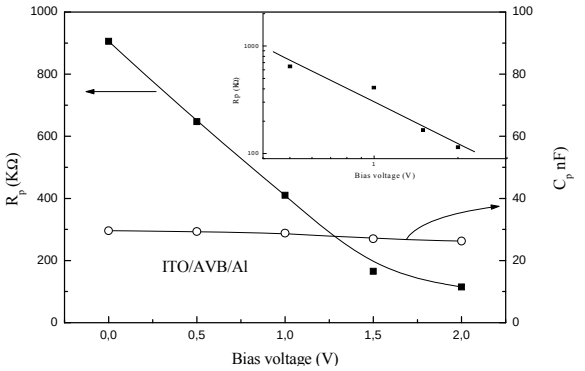

Fig. 9. Variation of the fitting parameters capacitance C_p and resistance R_p with bias voltages. The inset log–log plot of R_p with applied bias voltages.

Therefore, the voltage dependence of the R_p is given by [40]:

$$R_p \propto V / J \propto V^{-m}, \quad (15)$$

To determine the properties of the trap distribution in our devices, we represent in inset Fig. 9 the variation of R_p with V in a log–log scale. For two devices, a linear variation of the parallel resistance versus voltage (with m =1.28 for AVB and m =1 for AV2B) implies that conductance of the hole in anthracene thin film is consistent with an exponential trap distribution. The carriers may be trapped by structural defects or chemical impurities. Furthermore, the invariance of C_p with applied bias is well confirmed by the SCLC conditions. More detailed information about the transport properties of the device can be obtained by studying the different complex formalisms [30]. Each of which consists of real and imaginary components, namely

- Complex admittance, $Y^*(\omega) = Y' - jY'' = 1/R_p + jC_p\omega$;
- Complex modulus, $M^*(\omega) = M' - jM''$ and
- Complex permittivity, $\varepsilon^*(\omega) = \varepsilon' - j\varepsilon''$

4. Conclusions

We have studied a comparative study of dc current density–voltage (*J-V*) and ac impedance spectroscopy characteristics from two devices based ITO/anthracene derivatives/Al. For both the devices, charge carrier conduction is ohmic at lower bias and switches to the SCLC mechanism with an exponential trap distribution at a higher applied bias.

The impedance spectroscopy was showed that the sample can be modeled to a single parallel R_pC_p circuit with a small resistance R_s. The variation of conductivity with frequency and bias voltage was studied for ITO/anthracene derivative/Al devices. These features make the two new anthracene derivatives good candidates for optoelectronic applications.

References

[1]. R. H. Friend, R. W. Gymer, A. B. Holmes, J. H. Burroughes, R. N. Marks, C. Taliani, D. D. C. Bradley, D. A. Dos Santos, J. L. Brédas, M. Lögdlund, W. R. Salaneck, Electroluminescence in conjugated polymers, *Nature*, Vol. 397, pp. 121-128.

[2]. M. T. Bernius, M. Inbasekaran, J. O'Brien, W. Wu, Progress with Light-Emitting Polymers, *Advanced Materials*, Vol. 12, Issue 23, 2000, pp. 1737-1750.

[3]. X. Xu, G. Yu, Y. Liu, D. Zhu, Electrode modification in organic light-emitting, *Displays*, Vol. 27, Issue 1, 2006, pp. 24-34.

[4]. D. Kumaki, T. Umeda, T. Suzuki, S. Tokito, High-mobility bottom-contact thin-film transistor based on anthracene oligomer, *Organic Electronics*, Vol. 9, Issue 5, 2008, pp. 921-924.

[5]. N. Wang, J. Yu, Y. Zang, J. Huang, Y. Jiang, Effect of buffer layers on the performance of organic photovoltaic cells based on copper phthalocyanine and C60, *Solar Energy Materials and Solar Cells*, Vol. 94, Issue 2, 2010, pp. 263-266.

[6]. L. L. Chen, W. L. Li, H. Z. Wei, B. Chu, B. Li, Organic ultraviolet photovoltaic diodes based on copper phthalocyanine as an electron acceptor , *Solar Energy Materials and Solar Cells*, Vol. 90, Issue 12, 2006, pp. 1788-1796.

[7]. M. Pope, H. P. Kallmann, P. Magnante, Electroluminescence in Organic Crystals, *Journal of Chemical Physics*, Vol. 38, Issue 8, 1963, pp. 2042-2044.

[8]. M. G. Shin, S. O. Kim, H. T. Park, S. J. Park, H. S. Yu, Y. H. Kim, S. K. Kwon, Synthesis and characterization of ortho-twisted asymmetric anthracene derivatives for blue organic light emitting diodes (OLEDs), *Dyes Pigments*, Vol. 92, Issue 3, pp. 1075-1082.

[9]. P. S. Vincett, W. A. Barlow, R. A. Hann, G. G. Roberts, Electrical conduction and low voltage blue electroluminescence in vacuum-deposited organic films, *Thin Solid Films*, Vol. 94, Issue 2, 1982, pp. 171-183.

[10]. R. Ben Chaâbane, N. Jaballah, M. Benzarti-Ghédira, A. Chaieb, M. Majdoub, H. Ben Ouada, Synthesis and thin films characterization of new anthracene-core molecules for opto-electronic applications, *Physica B: Condensed Matter*, Vol. 404, Issue 14–15, 2009, pp. 1912-1916.

[11]. E. Gondek, I. V. Kityk, A. Danel, Some anthracene derivatives with N,N-dimethylamine moieties as materials for photovoltaic devices, *Materials Chemistry and Physics*, Vol. 112, Issue 1, 2008, pp. 301-304.

[12]. P. Raghunath, M. Ananth Reddy, C. Gouri, K. Bhanuprakash, V. Jayathirtha Rao, Electronic Properties of Anthracene Derivatives for Blue Light Emitting Electroluminescent Layers in Organic Light Emitting Diodes: A Density Functional Theory Study, *The Journal of Physical Chemistry A*, Vol. 110, 2006, pp. 1152-1162.

[13]. L. Valentini, D. Bagnis, A. Marrocchi, M. Seri, A. Taticchi, J. M. Kenny, Novel Anthracene-Core Molecule for the Development of Efficient PCBM-Based Solar Cells, *Chemistry of Materials*, Vol. 20, 2008, pp. 32-34.

[14]. D. A. M. Egbe, S. Turk, S. Rathgeber, F. Kuhnlenz, R. Jadhav, Anthracene Based Conjugated Polymers: Correlation between π-π-Stacking Ability, Photophysical Properties, Charge Carrier Mobility, and Photovoltaic Performance, *Macromolecules*, Vol. 43, 2010, pp. 1261-1269.

[15]. R. Ben Chaâbane, M. Gamoudi, G. Guillaud, C. Jouve, F. Gaillard, R. Lamartine, Elaboration and characterization of thin calixarene films, *Synthetic Metals*, Vol. 66, Issue 1, 1994, pp. 49-54.

[16]. K. C. Kao, W. Hwang, Electrical Transport in Solids, New York, *Oxford Pergamon Press*, 1981.

[17]. M. Pope, C. E. Swenberg, Electronic Processes in Organic Crystals, New York, *Oxford University Press*, 1982.

[18]. F. Michelotti, F. Borghese, M. Bertolotti, E. Cianci, Alq3/PVK heterojunction electroluminescent devices, *Synthetic Metals*, Vol. 111–112, 2000, pp 105-108.

[19]. Ma, I. A. Hümmelgen, X. Jing, Z. Hong, L. Wang, X. Zhao, F. Wang, F. E. Karasz, Charge transport in a blue-emitting alternating block copolymer with a small spacer to conjugated segment length ratio, *Journal of Applied Physics*, Vol. 87, 2000, pp. 312-317.

[20]. W. Brütting, S. Berleb, A. G. Mückl, Space-charge limited conduction with a field and temperature dependent mobility in Alq light-emitting devices, *Synthetic Metals*, Vol. 122, Issue 1, 2001, pp. 99-104.

[21]. R.G. Kepler, Charge Carrier Production and Mobility in Anthracene Crystals, *Physical Review*, Vol. 119, Issue 4, 1960, pp. 1226-1229.

[22]. G. Horowitz, Organic Field-Effect Transistors, *Advanced Materials*, Vol. 10, Issue 5, 1998, pp. 365-377.

[23]. A. Moliton, W. Rammel, B. Lucas, Field and temperature effects on the electronic mobility in Alq3 structures, *The European Physical Journal - Applied Physics*, Vol. 33, Issue 3, 2006, pp. 175-182.

[24]. M. Bajpai, K. Kumari, R. Srivastava, M. N. Kamalasanan, R. S. Tiwari, S. Chand, Electric field and temperature dependence of hole mobility in electroluminescent PDY 132 polymer thin films, *Solid State Communications*, Vol. 150, Issue 13–14, 2010, pp. 581-584.

[25]. A. Moliton, Optoélectronique moléculaire et polymère: des concepts aux composants, *Springer-Verlag*, Paris, 2003.

[26]. C. C. Chen, B. C. Huang, M. S. Lin, Y. J. Lu, T. Y. Cho, C. H. Chang, Impedance spectroscopy and equivalent circuits of conductively doped organic hole-transport materials, *Organic Electronics*, Vol. 11, Issue 12, 2010, pp. 1901-1908.

[27]. C. K. Suman, J. Yun, S. Kim, S. D. Lee, C. Lee, AC impedance spectroscopic studies of transport properties in metal oxide doped α-NPD, *Current Applied Physics*, Vol. 9, Issue 5, 2009, pp. 978-984.

[28]. A. K. Jonscher, Electronic properties of amorphous dielectric films, *Thin Solid Films*, Vol. 1, Issue 3, 1967, pp. 213-234.

[29]. E. Logakis, Ch. Pandis, V. Peoglos, P. Pissis, J. Pionteck, P. Pötschke, M. Mičušík, M. Omastová, Electrical/dielectric properties and conduction mechanism in melt processed polyamide/multi-walled carbon nanotubes composites, *Polymer*, Vol. 50, Issue 21, 2009, pp. 5103-5111.

[30]. H. Böttger, V. V. Bryksin. Hopping Conduction in Solids, Weinheim, *VCH Verlagsgesellschaft*, 1985.

[31]. A. K. Jonscher, The universal dielectric response, *Nature*, Vol. 267, 1977, pp. 673-679.

[32]. J. C. Dyre, T. B. Schrøder, Universality of ac conduction in disordered solids, *Reviews of Modern Physics*, Vol. 72, Issue 3, 2000, pp. 873-892.

[33]. K. M. Jager, D. H. McQueen, I. A. Tchmutin, N. G. Ryvkina, M. Kluppel, Electron transport and ac electrical properties of carbon black polymer composites, *Journal of Physics D: Applied Physics*, Vol. 34, 2001, pp. 2699-2707.

[34]. J. R. Macdonald, Impedance Spectroscopy-Emphasizing Solid Materials and Systems, New York, *Wiley-lnterscience*, 1987.

[35]. S. H. Kim, K. H. Choi, H. M. Lee, D. H. Hwang, L. M. Do, H. Y. Chu, T. Zyung, Impedance spectroscopy of single- and double-layer polymer light-emitting diode, *Journal of Applied Physics*, Vol. 87, Issue 2, 2000, pp. 882-889.

[36]. A. K. Jonscher, Dielectric Relaxation in Solids, London: Chelsea, *Dielectrics Press*, 1983.

[37]. A. Rouis, C. Dridi, R. Ben Chaabane, J. Davenas S. Aeiyach, H. Ben Ouada, Optical and electrical study of chromogenic calix[4]arene derivatives, *Materials Science and Engineering C*, Vol. 26, Issue 2–3, 2006, pp. 240-246.

[38]. J. Campbell, D. D. C. Bradley, D. G. Lidzey. Space-charge limited conduction with traps in poly(phenylene vinylene) light emitting diodes, *Journal of Applied Physics*, Vol. 82, Issue 12, 1997, pp. 6326-6343.

[39]. J. H. Ahn, H. S. Lee, D. S. Seo, K. U. Jang, W. J. Lee, T. W. Kim, Dielectric properties depending on frequency in organic light-emitting diodes, *Thin Solid Films*, Vol. 516, Issue 9, 2008, pp. 2626-2629.

[40]. M. A. Lampert, P. Mark, Current Injection in Solids, New York, *Academic Press*, 1970.